Design and Manufacturing of an Affordable Soft-Robotic Manipulator for Minimally Invasive Diagnosis

Vani Virdyawan
Faculty of Mechanical and Aerospace Engineering
Institut Teknologi Bandung
Bandung, 40132, Jawa Barat, Indonesia
virdyawan@ftmd.itb.ac.id

Tutla Ayatullah
Faculty of Mechanical and Aerospace Engineering
Institut Teknologi Bandung
Bandung, 40132, Jawa Barat, Indonesia
tutla@ftmd.itb.ac.id

Arif Sugiharto
Faculty of Mechanical and Aerospace Engineering
Institut Teknologi Bandung
Bandung, 40132, Jawa Barat, Indonesia
arif.sugiharto@itb.ac.id

Enrico Franco
The Mechatronics in Medicine Laboratory, Mechanical Engineering Department
Imperial College London
London, SW7 2AZ UK
ef1311@imperial.ac.uk

Arnau Garriga-Casanovas
The Mechatronics in Medicine Laboratory, Mechanical Engineering Department
Imperial College London
London, SW7 2AZ UK
a.garriga-casanovas14@imperial.ac.uk

Andi Isra Mahyuddin
Faculty of Mechanical and Aerospace Engineering
Institut Teknologi Bandung
Bandung, 40132, Jawa Barat, Indonesia
aim@ftmd.itb.ac.id

Ferdinando Rodriguez y Baena
The Mechatronics in Medicine Laboratory, Mechanical Engineering Department
Imperial College London
London, SW7 2AZ UK
f.rodriguez@imperial.ac.uk

Indrawanto
Faculty of Mechanical and Aerospace Engineering
Institut Teknologi Bandung
Bandung, 40132, Jawa Barat, Indonesia
indrawanto@ftmd.itb.ac.id

***Abstract*—Soft robotic manipulators are inherently compliant thus they are ideally suited for minimally invasive diagnosis and intervention. In addition, soft robotics allows for affordable manufacturing, thus it could be adopted in low and middle-income countries where conventional robotics is prohibitively expensive. In this work, the design, manufacturing, and actuation strategy of an affordable soft robotic manipulator is presented. The manufacturing process does not rely on sophisticated technologies, and the pneumatic actuation does not require digital pressure regulators. Instead, a low-cost solution consisting of a needle valve operated by a servo motor is employed. The prototype is assessed with experiments that demonstrate its functionality.**

Keywords—soft robots, surgical robot, endotracheal intubation, affordable pneumatic actuation method, minimally invasive surgery

I. INTRODUCTION

Endotracheal intubation (ETI) is a very common emergency procedure, but it has a high risk of complications [1]. Existing instruments for ETI only bend in one direction thus they need to be rotated manually around their axis to align with the upper airways. This operation is conducted routinely by clinicians, but it bears the risk of injuries. Recently, ETI has been employed increasingly for infectious respiratory diseases. For instance, approximately 3% of COVID-19 patients required ETI as part of their treatment [2]. Due to the infectious nature of COVID-19, clinicians are required to wear the highest level protective equipment available, which makes the procedure more difficult [3]. Low and middle income countries (LMIC) have a particularly high incidence of infectious respiratory diseases, including tuberculosis (TB). In Indonesia for example, there are over one million new cases of TB every year [4].

A number of devices have been developed for ETI, such as [5], which employs a tendon driven actuator and has an outside diameter of 7.1 mm. Another example is [1], which has two degrees of freedom (DOFs) and is also actuated by tendons. However, the manufacturing process for these systems is complex, and the devices might not be suitable for single use. Another method to perform ETI relies on using a flexible bronchoscope, but it is not financially viable in LMIC. In this respect, soft robots represent an attractive. alternative due to their low cost, bio-compatibility, and intrinsic safety in unstructured environments [6]. For instance, [7] proposed a soft manipulator for bronchoscopy which consists of two actuators, one for twisting and one for bending, and has an outer diameter of 6.5 mm. A soft manipulator with 2.4 mm outer diameter was proposed in [8]. However, the latter system only has one DOF and it is intended to be used in conjunction with conventional bronchoscopes. In summary, further effort is required to develop an affordable instrument for ETI which can be produced locally in LMIC.

In this work we present a soft continuum manipulator with two actuated DOFs, that is i) bending on an arbitrary plane; ii) rotation of the bending plane with respect to a fixed reference frame (see Fig. 1). The design is based on the framework outlined in our previous work [9], and on the requirements for ETI presented in [1]. The main contributions of this work include the following points: i) a low cost embodiment of the design outlined in [9], which offers higher force than other soft

This work was supported by a Newton Fund Institutional Links grant, ID 623531377, under the Newton Fund Indonesia partnership. The grant is funded by the UK Department for Business, Energy and Industrial Strategy and Directorate of Resources Affairs Directorate General of Higher Education Ministry of Education, Culture, Research and Technology, Republic of Indonesia, contract no: 341/E4.1/AK.04.PT/2021 and 083/E5/PG.02.00.PT/2022, and delivered by the British Council.

robots for a given diameter as shown in [10]; ii) a manufacturing process which only relies on resources available in LMIC is outlined; iii) an affordable pneumatic actuation system consisting of a needle valve operated by a servo DC motor is employed instead of sophisticated digital pressure regulators, which are frequently used in soft robotics; iv) the prototype is assessed with extensive experiments to demonstrate its functionality.

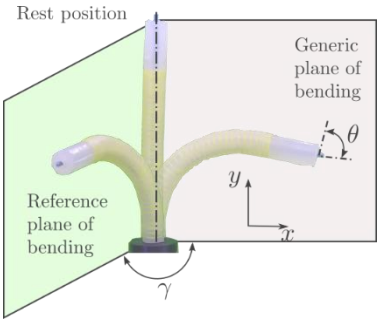

Fig. 1. Two DOFs of the soft manipulator prototype: bending on a plane θ; orientation of the bending plane γ with respect to a fixed reference frame

The rest of the paper is organised as follows. Section II details the design and the manufacturing of the soft manipulator. Section III presents the pneumatic actuation. Section IV presents the experimental results. Section V contains concluding remarks and suggestions for future work.

II. Design and Manufacturing

The soft manipulator is designed following the principles and morphing design features in [9] to maximise its force while maintaining a small diameter and accommodating payload. The manipulator is tubular, with a constant cross section made of three partition walls that define three internal chambers spaced at 120° to allow bending on any plane. The entire cross section and partition walls are made of silicone, so that it can easily deform when pressurised. This creates a morphing structure where the pressurised chambers expand to occupy practically all the cross section, which maximises the pressurised chamber area and maximises the distance between the center of pressures and center of tensions in the cross section. The result is a morphing design that has higher force than any other soft robotic manipulator, as shown in [10].

The silicone-rubber material employed for manufacturing is Dragon Skin™ 10 Medium (Smooth-On, Inc., Pennsylvania, USA), which provides a good compromise between compliance and mechanical properties (i.e. ability to withstand pressures up to 1.5 bar with the current design). Elastosil 4601M supplied by Wacker Chemie AG, Germany, can provide even higher force since it can withstand higher pressures, as shown in [10], but it is not available in some LMIC such as Indonesia, and is therefore not used. An inextensible cable sleeve is placed at the center of the section to prevent elongation when the chambers are pressurized, thus increasing the maximum bending and force at any given pressure. In future work, the cable sleeve will host an endoscopic camera. A second thread is wound around the external cylindrical surface to prevent radial expansion. The outer diameter of the manipulator is 6 mm, which is similar to [1], and the length is approximately 55 mm, which is comparable to the length of the bending section in commercially available bronchoscopes.

The manufacturing process consists of three main steps. Initially, silicone-rubber is injected using a syringe pump in a four-part mould consisting of a two-part outer mould, an inner mould, and a base mould (see Fig. 2a). The outer moulds were manufactured using a conventional 3D printer (Objet500, Stratasys, Ltd., Israel), while the inner mould was manufactured using a metal 3D printer (Renishaw AM250, Renishaw plc, UK). A tungsten-carbide rod is placed along the axis of the mould to produce the central working channel in the prototype. To avoid misalignment, the different parts of the mould are aligned using locating pins. Instead of employing a vacuum chamber, a bespoke syringe pump was developed to degas the silicone-rubber (Fig. 2b). The main advantage of this approach is that the degassed silicone rubber can be injected directly in the mould without transferring it to a different syringe, which would be required if a vacuum chamber was used. This helps to minimize the occurrence of bubbles which might affect the integrity of the prototype. The main limitation of this method lies in the maximum amount of silicone-rubber that can be injected by a given syringe pump. Thus, the syringe pump should be sized according to the dimensions of the prototype.

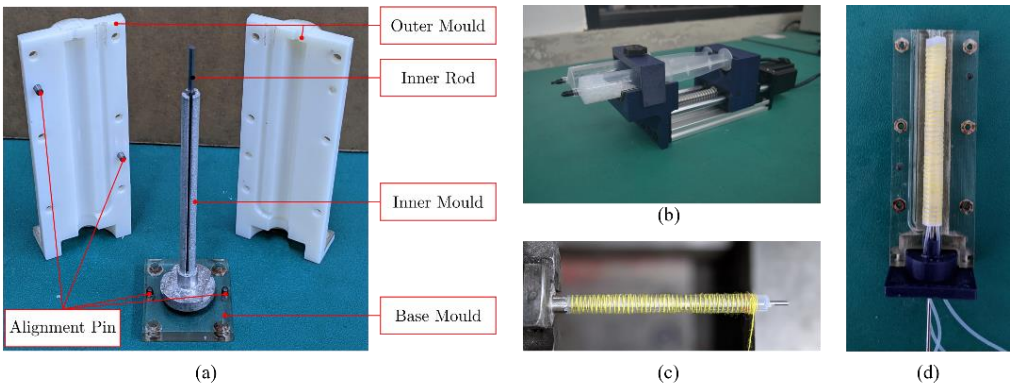

Fig. 2. a) Moulds employed to manufacture the prototype; b) syringe pump employed for degassing and injection of silicone-rubber; c) thread winding process using a lathe machine (performed before removing the inner mould); d) the prototype is inserted into the mould and positioned above the silicone injection channel in order to seal the ends of the internal chambers

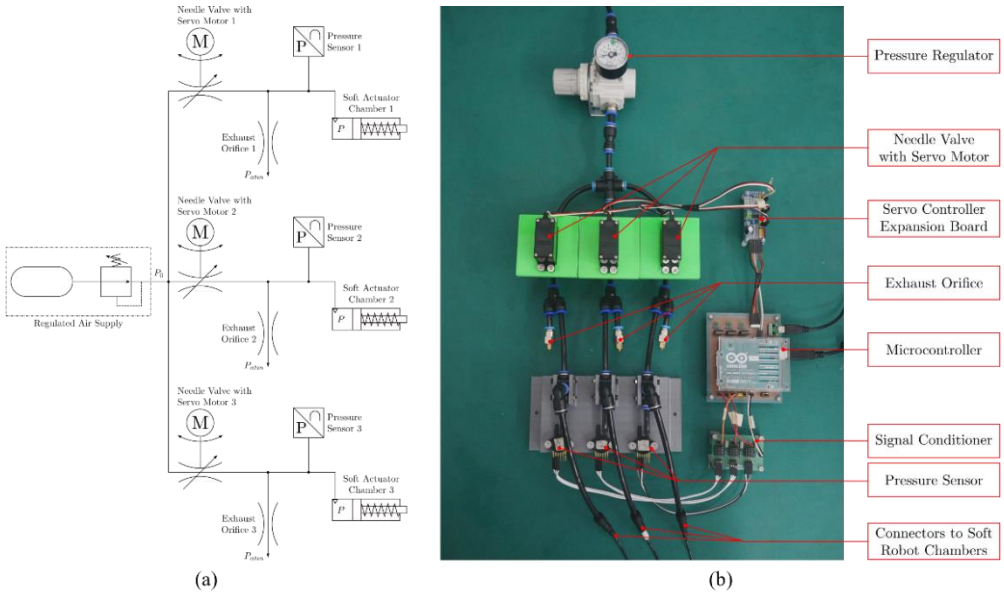

Fig. 3. a) Schematic of the affordable pneumatic actuation system; b) prototype with key components.

After casting the silicone-rubber in the mould, an inextensible thread is wound around the outer face of the prototype using a lathe machine, while the inner mould is kept in place to prevent deformation (Fig. 2c). Employing a lathe allows winding the thread with a regular pitch in both directions (i.e. clockwise and counterclockwise), which helps to prevent twisting effects [11]. In this work we employed a 1.5 mm pitch in both winding directions (e.g. larger pitches can result in ballooning between the threads, while smaller pitches bear the risk of overlaying different threads leading to impingement). Subsequently, the external mould is mounted back on the prototype and the external threads are enclosed with a second casting of silicone-rubber. Finally, one end of the prototype is sealed with silicone-rubber, while silicone tubes are connected to the other end. At this stage the prototype is inserted into the outer mould, and a different base is used to accommodate the routing of the silicone tubes (see Fig. 2d). In particular, the prototype is located above the silicone injection channel to ensure that all the chambers are fully sealed. At this stage, the inextensible cable sleeve is inserted in the working channel of the manipulator. Silicone tubes are employed to facilitate bonding with the mould and to allow pressurizing the internal chambers.

III. Affordable Pneumatic Actuation

The internal chambers of the manipulator are pressurized using a needle valve (part number 7770 06 00, Legris) operated by a servo motor (Servomotor RC 6V, Parallax Inc, CA, USA), while a fixed flow restrictor with an orifice diameter of 0.6 mm (MK8 Nozzle, Shenzhen Creality 3D Technology Co., Ltd, China) serves as exhaust valve (Fig. 3b). When the servo motor opens the needle valve, the flow rate to the internal chamber increases resulting in a pressure increment. Conversely, when the servo motor closes the needle valve, the chamber is vented through the exhaust valve and the internal pressure drops [12]. The pressures P_1, P_2, P_3 in the internal chambers cause the manipulator to bend on a plane according to [11].

TABLE I. First Order Approximation of the Open-Loop Pressure Transient Response

Parameter	Servo Angle (°)			
	40	80	120	140
K (bar/°)	0.004	0.006	0.006	0.007
τ (s)	0.074	0.136	0.195	0.237
t_d (s)	0.194	0.235	0.267	0.288

Therefore, at equilibrium and in the absence of external forces we have.

$$\theta = 1/k\sqrt{P_3^2 + P_1^2 + P_2^2 - P_1P_2 - P_1P_3 - P_2P_3} \quad (1)$$

$$\tan(\gamma) = \sqrt{3}(P_1 - P_2)/(P_1 + P_2 - 2P_3) \quad (2)$$

where θ is the tip rotation on the bending plane, γ is the orientation of the bending plane with respect to a fixed reference frame, and k is the structural stiffness of the manipulator, which can be nonlinear.

An expansion board is employed to control the servo motors (PCA9685, Adafruit Industries, NY, USA) and communicates with the microcontroller (Arduino Uno) using an I2C protocol. The pressures relative to atmosphere are measured with analog pressure sensors (MPX5500DP, NXP Semiconductors N.V., Netherlands). The pressure signals are sampled at 100 Hz and are filtered using an active lowpass filter with a cut-off frequency of 48 Hz to avoid aliasing, while a voltage follower is employed to stabilize the values. The measurement were calibrated by comparing the output voltage of the sensors with the reading of a pressure gauge (MAP 40-4-1/8-EN, Festo SE & Co. KG, Germany). The procedure involved increasing the pressure in 0.05 bar increments from 0 bar to 4 bar (see Section IV).

A manual pressure regulator is employed to set the supply pressure to the constant value P_0 = 4 bar. To avoid damaging the manipulator, the orifice size of the exhaust valves were

chosen such that the absolute pressure in the internal chambers remains always below 2 bar.

IV. Experimental Results

A. Pneumatic Actuation

To ascertain that the proposed actuation system can be used as a proportional pressure regulator, we investigated experimentally the relationship between the angle of the servo motor and the output pressure in open loop. In this set of experiments, the pneumatic actuation system was connected to a pressure gauge rather than to the manipulator. A normalized signal between 0 and 1 that corresponds to the position of the servo motor between 180° (i.e. yielding the maximum pressure) and 0° (i.e. yielding the minimum pressure) was communicated to the microcontroller. The results are shown in Fig. 4a, which represents the steady state pressure values for different servo angles.

The minimum achievable pressure corresponding to 0° servo angle is 0.2 bar rather than 0 bar, since the needle valve requires more than 180° to fully open and fully close. Nevertheless, the prototype does not bend at 0.2 bar hence this value is acceptable for our system. Setting P_0 at 4 bar, the maximum pressure achievable is 1.5 bar with the chosen exhaust orifice. This value can be further increased by reducing the size of the exhaust orifice, however the minimum pressure would then also increase. The relationship between pressure and servo angle is nonlinear and is characterized by hysteresis. This behaviour can be explained by considering that an angular movement of the servo yields an axial movement of the needle hence the equivalent orifice size changes in a nonlinear fashion. In addition, the servo motor has a non-negligible dead-band which could result in angular errors for small movements due to friction. As a result, the valve conductance, which is proportional to the size of the equivalent orifice, also undergoes a nonlinear variation. In turn, the mass flow rate from the needle valve, which in isothermal and choked flow conditions can be expressed as $Q = CP_0\rho_0$, where C is the conductance of the orifice and ρ_0 the density of the gas, also varies in a nonlinear fashion. The pressure dynamics can be expressed as [12]

$$\dot{P} = -P\dot{V}/V + (Q_{in} - Q_{out})R_sT/V \quad (3)$$

where Rs is the specific gas constant, V is the volume of the gas (i.e. constant in this test), the incoming flow rate Q_{in} depends on the position of the servo, and Q_{out} is the outflow from the exhaust valve.

The transient response of the open loop system is shown in Fig. 4b and can be approximated as a first-order system with three parameters: steady-state gain (K), time constant (τ), and time delay (t_d). The value of the parameters are given in Table I. The time constant and the time delay increase with the servo angle, since a larger movement of the servo is required. The servo motor has a maximum speed of 140 rpm at no-load, and a 180° rotation takes approximately 0.7 seconds when the motor shaft is attached to the needle valve. Notably, all curves increase with a similar slope. These results can be explained considering that the needle valve experiences chocked flow conditions, thus the speed of the air flow is equal to the speed of sound.

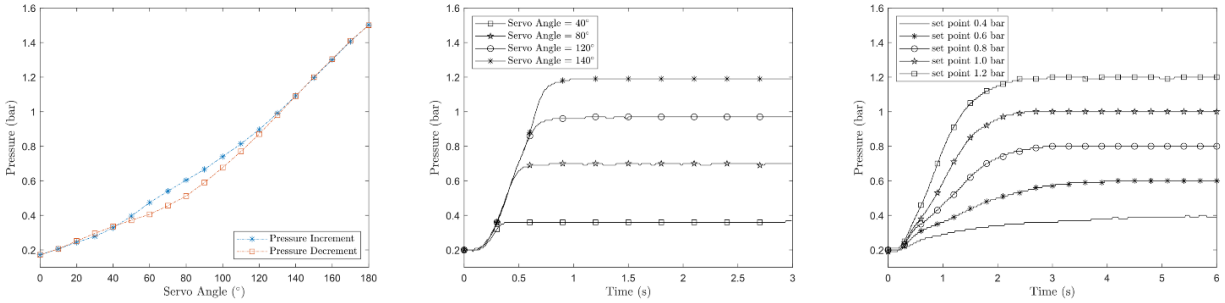

(a) (b) (c)

Fig. 4. a) Relationship between angle of the servo motor and output pressure of the pneumatic actuation system; b) open-loop step response of the output pressure for different servo angles; c) close-loop step responses of the output pressure with a PI controller.

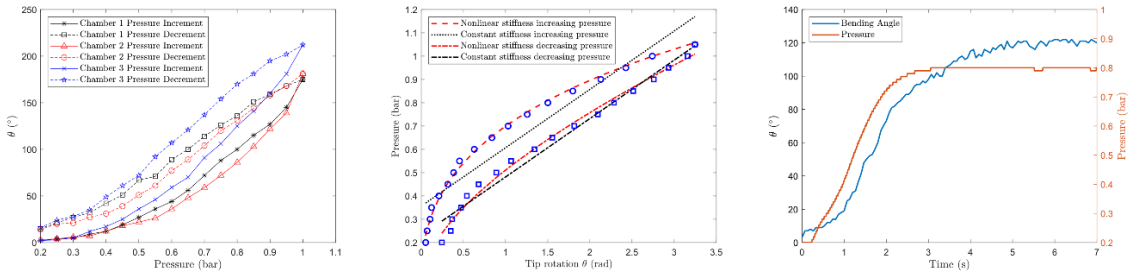

(a) (b) (c)

Fig. 5. a) Relationship between bending angle (θ) and regulated pressure P for each chamber; b) stiffness models for chamber 3 during pressurization and depressurisation; c) transient response of the bending angle θ and of the corresponding pressure P with a pressure set-point of 0.80 bar

TABLE II. STIFFNESS MODEL PARAMETERS

Chamber #	Pressurisation			Depressurisation		
	k_0	k_1	k_2	k_0	k_1	k_2
1	0.08	0.57	0.29	0.21	0.24	0.27
2	0.10	0.57	0.25	0.07	0.44	0.49
3	0.07	0.52	0.27	0.15	0.27	0.30

Closed-loop experiments were conducted to characterize the pneumatic actuation as a single block. For illustrative purposes, a PI algorithm was employed to regulate the output pressure P to prescribed values between 0.4 bar and 1.2 bar with a 0.2 bar increment.

The controller parameters were tuned empirically as K_p = 20 and K_i = 150 to avoid overshoot. This approach is similar to commercially available proportional pressure regulators [13]. The transient response of the closed loop system is shown in Fig. 4c. Differently from the open loop system, the time constant decreases with the pressure set-point. This is expected considering that a larger pressure results in a higher flow rate with the same orifice size. With the tuning employed, the closed loop system is slower than the open loop system in reaching the steady state condition.

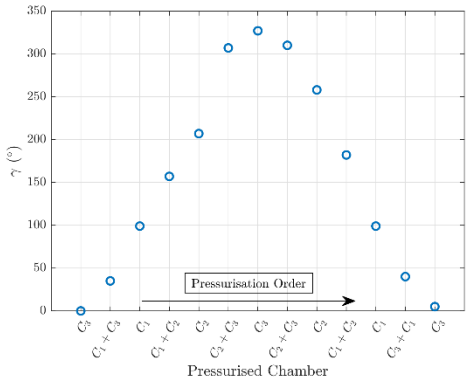

Fig. 6. Orientation of the bending plane when the chambers are pressurized in sequence. The value of is relative to the bending plane of C_3.

In summary, the results indicate that the proposed pneumatic actuation can effectively regulate the output pressure in a range appropriate for our soft manipulator. Similarly to commercially available proportional valves, the proposed system also exhibits a first-order transient, but it is characterized by a slower responsiveness, which is limited by the speed of the servo motor. Notably, the cost of the components is approximately $50, which is one order of magnitude smaller than commercially available digital pressure regulators. Thus, provided that fast responsiveness is not paramount for the application, the proposed actuation system represents a viable solution for LMIC, where high equipment cost remains a barrier to research and innovation.

B. Prototype Characterization

Using the pneumatic actuation system described in Section IV-A, the relationship between the bending angle θ of each chamber with its internal pressure P was investigated. The measurements were performed with a digital camera (GoPro Hero5, GoPro, Inc., California, USA) as follows: i) the direction of the z-axis was initially defined; ii) the bending angle θ was then measured with respect to the z-axis (see Fig. 1) while the pressure was increased between 0.20 bar and 1.00 measurements were repeated while decreasing the pressure from 1.00 bar to 0.20 bar with 0.05 bar decrements.

At a pressure of 1 bar, the manipulator has a bending angle of 175°,181°, and 212° for chamber 1, chamber 2, and chamber 3, respectively. These values are comparable with those of commercially available bronchoscopes, which typically provide a maximum bending angle of 180° (e.g., Ambu® aScope™ 4 Broncho Regular, Ambu A/S, Denmark). The relationship between pressure P and angle θ for each chamber is shown in Fig. 5a. Chamber 1 and chamber 2 show similar characteristics, while chamber 3 has larger bending angles with the same internal pressure. We postulate that this difference could be due to the different internal geometry of the chambers. The inner mould has a high aspect ratio (i.e. length / diameter = 13) and was manufactured with a metal 3D printer that employs a selective laser melting (SLM) technology. Such geometry is however difficult to produce with an SLM 3D printer and might result in dimensional inaccuracies. In addition, the hysteresis observed between pressurisation and depressurisation can be attributed to the inextensible cable sleeve placed at the centre of the section, which tends to keep its shape when deformed. This effect could be minimized by changing the material of the cable sleeve, or it could be compensated by using an appropriate closed-loop control strategy. Both options will be investigated as part of our future work. In addition, we will develop a new mould that can be manufactured using conventional manufacturing processes widely available in LMIC, which might also result in higher dimensional accuracy.

The structural stiffness of the manipulator corresponding to each chamber can be modelled using a fractional order polynomial as $k = k_0 + k_1\theta^{k2}$ [14], which provides a better approximation compared to a constant stiffness model (see Fig. 5b). The values of k_0, k_1 and k_2 for each chamber during pressurisation and depressurisation are given in Table II. The stiffness parameters during pressurisation are similar for all chambers. Conversely, a wider variation is observed during depressurisation. This occurs since pressurization starts from the rest condition with the prototype in a straight configuration. Instead, the initial condition for depressurization is different for different chambers. Thus, the hysteresis due to the inextensible cable sleeve results in different stiffness parameters.

The transient response of the bending angle θ and of the corresponding input pressure are shown in Fig. 5c. The pressure set-point was set at 0.8 bar for illustrative purposes. The transient response of the bending angle can also be approximated as a first order system with K = 155.4 °/bar, τ = 1.44 s, and t_d = 0.75 s. As expected, θ has a slower dynamics compared to the input pressure (time constant 1.44 s, and 0.95 s for θ and pressure, respectively). Considering that steady-state accuracy is typically more important for minimally invasive diagnosis and surgery compared to responsiveness, the results suggest that the system dynamics could be suitable for this type of applications.

In order to measure the orientation of the bending plane γ, the experimental setup was modified by moving the camera

above the prototype. Pressurizing chamber 1 (i.e C_1), chamber 2 (i.e C_2), and chamber 3 (i.e C_3) individually resulted in γ = 136°, γ = 241°, and γ = 0° respectively, which broadly correspond to the geometry of the internal chambers (i.e., spaced at 120°). This suggests that, in the absence of position sensors, the manipulator could be operated by controlling the pressure in the internal chambers with the proposed actuation system and by setting P^* correspo nding to the desired orientation $(\theta,\gamma) = (\theta^*,\gamma^*)$ based on training data. In this experiment, the value of γ is relative to the bending plane corresponding to chamber 3. Subsequently, multiple chambers were pressurized simultaneously at 0.8 bar in the following order: $C_3 \rightarrow C_3 + C_1 \rightarrow C_1 \rightarrow C_1 + C_2 \rightarrow C_2 \rightarrow C_2 + C_3 \rightarrow C_3 \rightarrow C_2 + C_3 \rightarrow C_2 + C_1 \rightarrow C_1 \rightarrow C_1 + C_3 \rightarrow C_3$ (see Fig. 6b). After one complete cycle, the angle did not go back to its initial value corresponding to C3. This behaviour is also observed when reversing the pressurization sequence. Possible causes include: i) different internal geometry of the chambers, leading to one of them being dominant (e.g. Fig. 5a shows that chamber 3 results in a larger bending angle); ii) buckling of the internal wall when one of the chambers is pressurised (e.g. the direction of buckling depends on the bending angle as well as on the pressure in the adjacent chambers); iii) the cable sleeve partially retains its shape when deformed and might result in a preferred bending direction.

V. Conclusion

In this work we presented the design and manufacturing of an affordable soft manipulator that could be used for minimally invasive diagnosis. Compared to other solutions that employ rigid robots, a soft manipulator can provide a safer alternative due to its inherent compliance. A manufacturing process that employs equipment available in LMIC was outlined. In addition, an affordable pneumatic actuation system was proposed in order to replace more sophisticated and expensive digital pressure regulators. The experimental results indicate that the actuation system can be employed as a regulated pressure source, provided that fast response is not paramount. The experiments on the prototype indicate that the range of motion is comparable to that of commercially available bronchoscopes. The study also highlighted that the prototype is characterized by nonlinear stiffness, which is in a agreement with our prior research.

This study also has some limitations. First of all, the cable sleeve embedded along the axis of the prototype results in hysteresis and affects the stiffness characteristics of the manipulator. This effect is likely to arise again when the cable sleeve is replaced by a camera cable, and might become dominant due to the low stiffness of the silicone-rubber employed for manufacturing. To this end, further work is required to model the behaviour of this element and to account for it within an appropriate closed-loop controller. Secondly, a sensing method to measure the bending angles of the prototype and to close the control loop needs to be developed. Plausible options include shape sensing and visual servoing based on camera images. Finally, the system needs to be made washable or disposable, and its functionality should be verified in clinical settings. Future work will focus on these aspects with the aim to develop a fully functional system for ETI that can be deployed safely and affordably in LMIC.

References

[1] Q. Boehler, et al., "Realiti: A robotic endoscope automated via laryngeal imaging for tracheal intubation," *IEEE Transactions on Medical Robotics and Bionics*, vol. 2, no. 2, 2020.

[2] L. Meng, et al., "Intubation and ventilation amid the covid-19 outbreak: Wuhan's experience," *Anesthesiology*, vol. 132, no. 6, pp. 1317–1332, 2020.

[3] H. Zheng, et al., "Clinical experience with emergency endotracheal intubation in covid-19 patients in the intensive care units: a single-centered, retrospective, descriptive study," *American Journal of Translational Research*, vol. 12, no. 10, p. 6655, 2020.

[4] N. Mboi, et al., "On the road to universal health care in indonesia, 1990–2016: a systematic analysis for the global burden of disease study 2016," *The Lancet*, vol. 392, no. 10147, pp. 581–591, 2018.

[5] X. Cheng, et al., "Intubot: Design and prototyping of a robotic intubation device," in 2018 *IEEE International Conference on Robotics and Automation* (*ICRA*). IEEE, 2018, pp. 1482–1487.

[6] M. Runciman, A. Darzi, and G. P. Mylonas, "Soft robotics in minimally invasive surgery," *Soft robotics*, vol. 6, no. 4, 2019.

[7] R. F. Surakusumah, et al., "Development of a half sphere bending soft actuator for flexible bronchoscope movement," in *2014 IEEE International Symposium on Robotics and Manufacturing Automation* (*ROMA*), 2014, pp. 120–125.

[8] M. McCandless, A. Perry, N. DiFilippo, A. Carroll, E. Billatos, and S. Russo, "A soft robot for peripheral lung cancer diagnosis and therapy," *Soft Robotics*, 2021.

[9] A. Garriga-Casanovas, I. Collison, and F. Rodriguez y Baena, "Toward a common framework for the design of soft robotic manipulators with fluidic actuation," *Soft robotics*, vol. 5, no. 5, pp. 622–649, 2018.

[10] A. Garriga-Casanovas, et al., "Optimised design and performance comparison of soft robotic manipulators," *arXiv preprint*, arXiv:2209.03831, 2022.

[11] K. Suzumori, "Elastic materials producing compliant robots," *Robotics and Autonomous Systems*, vol. 18, no. 1-2, pp. 135–140, jul 1996.

[12] E. Franco, T. Ayatullah, A. Sugiharto, A. Garriga-Casanovas, and V. Virdyawan, "Nonlinear energy-based control of soft continuum pneumatic manipulators," *Nonlinear Dynamics*, pp. 1–25, sep 2021.

[13] E. Franco and A. Garriga-Casanovas, "Energy Shaping Control of Soft Continuum Manipulators with in-plane Disturbances," *The International Journal of Robotics Research*, vol. 40, no. 1, mar 2021.

[14] E. Franco, A. Garriga-Casanovas, J. Tang, F. R. y Baena, and A. Astolfi, "Adaptive energy shaping control of a class of nonlinear soft continuum manipulators," *IEEE Transactions on Mechatronics*, 2021.